First order simulations on time measurements using inorganic scintillators for PET applications

Baptiste Joly, Gerard Montarou, N. Pauna

First order simulations on time measurements using inorganic scintillators for PET applications

B. Joly, G. Montarou, N. Pauna

Laboratoire de Physique Corpusculaire de Clermont Ferrand
IN2P3/CNRS Université Blaise Pascal
F-63177 Aubière Cedex, France

Abstract

Time measurements based on scintillating crystals are used in many different experimental sets-up in high energy physics, nuclear physics and medical imaging (e.g. PET). Time of Flight (TOF) positron emission tomography (PET) is based on the measurement of the difference between the detection times of the two gamma arising from positrons decays. The fundamental improvement of TOF is an increase in signal to noise ratio which translates into sensitivity improvement.

Conventional method for time measurements is based on the detection of first photoelectrons. Recently, in LHC experiments and more particularly for electromagnetic calorimeter, a fully digital method based on optimal filtering that considers samples of the entire signal was successfully applied. Since such a method allows ultimately time resolutions of about a few tens of picoseconds, for this report , first order simulations were performed using a simplified model of a detection block made of a PMT coupled to a LYSO or $LaBr_3$ crystal. These simulations were achieved to estimate time resolutions with the conventional method (first photoelectrons detection with CFD) or the optimal filtering. A hybrid method is also tested to be applied with fast running front-end electronics. These simulations will be the basis for experimental future studies.

Key-words: γ detection - time measurement - simulations - optimal filtering

PCCF RI 0702

Contents

1 Introduction

The detection method for gamma radiation based on scintillating crystals has been used in many fields from a long time. In particular, in medical imaging field, it is used for PET camera where the detection of two coincident low energy gamma is required.

PET detectors are similar to calorimeters of High Energy Physics (HEP) experiments. The events selection is different but the aim is the same: the estimation of time and energy. One of the important differences between HEP and medical imaging field is the radiation energy range: it is an important feature as it is also responsible for the photodetector signal quality.

A number of PET cameras incorporating TOF measurements have been built since the 1980s. Time-of-flight positron emission tomography is based on the measurement of the difference between the detection times of two gamma rays arising from the decay of a positron. The fundamental improvement brought by TOF is an increase in signal-to-noise ratio (SNR) which translates into sensitivity improvement High timing resolution has also the benefit that random coincidence event rates can be reduced as a narrower coincidence window can be used.

Conventional method for time measurements is based on the detection of first photoelectrons converted by the photodetector. With analogical method, arrival times of those first photoelectrons are measured with a constant fraction discriminator (CFD) or a leading edge discriminator.

Recently, Olcott et *al.* have developed a fully digital approach of a CFD [OLCOTT06]. With this CFD implementation, time measurements have been performed for coincident interactions of 511 keV photons of a Na22 source, with a LSO crystal coupled to fast PMT. Many tests have also been realized by Moszynski et *al.* in collaboration with Photonis [MOSZ03]. The last results of Szczesniak et *al.* for a 10x10x5 mm^3 LSO crystal coupled to a XP20D0 PMT indicate 215 ps (172 ps) measured (corrected) coincidence timing resolution [SZCZ06].

On the other hand, in HEP and more particularly for LHC calorimeter, a fully digital method based on optimal filtering that considers samples of the entire signal was applied. This approach allowed time resolutions about a few tens of picoseconds for some channels of the liquid argon electromagnetic calorimeter [NIKOLIC04].

Time measurement issue can be analyzed by these two different approaches: we can consider just one part of the signal for triggering on the first photoelectrons like in conventional methods or a larger part of the shaped signal for using optimal filtering. The first approach can be source of dead time; this can be reduced with a pipelined electronic of the sampled signal. Additionally, optimal filtering method has the advantage that information about arrival time and amplitude of the signal is simultaneously recovered.

In TOF PET application, the limitation on the ability to localize the positron annihilation point is mainly due to the uncertainty on the measured time difference t, which is related to the time resolution Δt of the coincidence system. This uncertainty is implemented in the reconstruction algorithm as a probability function for the localization of the detected annihilation: the events are located along the line of response (LOR) identified by the two detectors, its most probable position is set to the position corresponding to the measured TOF difference Δt, and the $fwhm$ of the probability function is the localization uncertainty $\Delta x(fwhm) = c\Delta t/2$.

The variance reduction is estimated by $2D/(c\Delta t)$, where D is the diameter of the object being imaged, c is the speed of light, and Δt is the coincidence timing measurement accuracy. This measurement allows us to localize the annihilation event along the LOR with a spatial resolution about 75-120 mm, assuming a time resolution of 500-800

ps. Good timing resolution gives additional spatial information to the reconstruction algorithms.

Recently, the introduction of new scintillators such as LSO and LaBr3 has reopened the interest of the research community in TOF PET. First clinical PET using TOF with a 650 ps time resolution had been produced and delivered to hospital by Philips. These TOF PET camera are based on analogical CFD method for timing measurement.

In this paper we performed first order simulation using a simplified model of a detection block made of a PMT coupled to LYSO or LaBr3 crystal. Time distribution of scintillating photons have been considered by taking into account only statistical fluctuations for timing resolution analysis with different methods: CFD, optimal filtering and a home-made hybrid method (Variable Fraction Discriminator).

In section 2 conventional time measurement methods with detection of the first photoelectrons will be simulated. Section 3 is devoted to optimal filtering method. In section 4 a hybrid reconstruction method is described. This algorithm is based on the detection of a variable fraction of the rising edge of the shaped signal. Perspectives are withdrawn in the last section of this study.

2 Detection of the k^{th} photoelectron. Timing with constant fraction discriminator

The accurate time measurement of photodetector signals by mean of a discriminator involves the detection of arrival time of the first photoelectrons. Several authors have derived the analytical expressions of the probability distribution of the k^{th} photon emission time from a crystal, out of a total number N of photons, N being either fixed or Poisson distributed with a mean value N_m.

Post and Schiff [POST50] derived first in 1950, the ultimate time performances with scintillators, assuming the expression (1) for the emission probability density of each photon, the scintillation starting at time $t = 0$

$$f(t) = 1/\tau \cdot e^{-t/\tau} = \lambda \cdot e^{-\lambda t} \tag{1}$$

In this document we will use $\lambda = 1/\tau$ for equations simplicity. The function $f(t)$ represents the evolution in time of scintillation light intensity. Emission time of photocathode photoelectrons are supposed to be distributed according to the same law.

The total number of photoelectrons emitted per event (photoelectric absorption or Compton scattering) is N. This number can be fixed to a constant value or randomly distributed according to a distribution function $p(n)$ (generally a Poisson law).

Figure 1 shows simulated events where the number of photoelectrons is fixed to 100, 2800 and 5600. The value 2800 is roughly equal to the emission from a 5x5x15 mm3 LSO crystal following detection of a 511 KeV gamma. The line represents the function $f(t) = 1/\tau \cdot e^{-t/\tau}$ with $\tau = 40ns$. It is obvious that the statistical fluctuations are reduced when the number of photoelectrons is high.

The detailed calculation of emission time distribution functions for the k^{th} photoelectron (k from 1 to N), is described in Appendix E. The integrated function of $f(t)$ is the cumulated distribution

$$F(t) = \int_0^t f(u)du = (1 - exp(-\lambda t)) \tag{2}$$

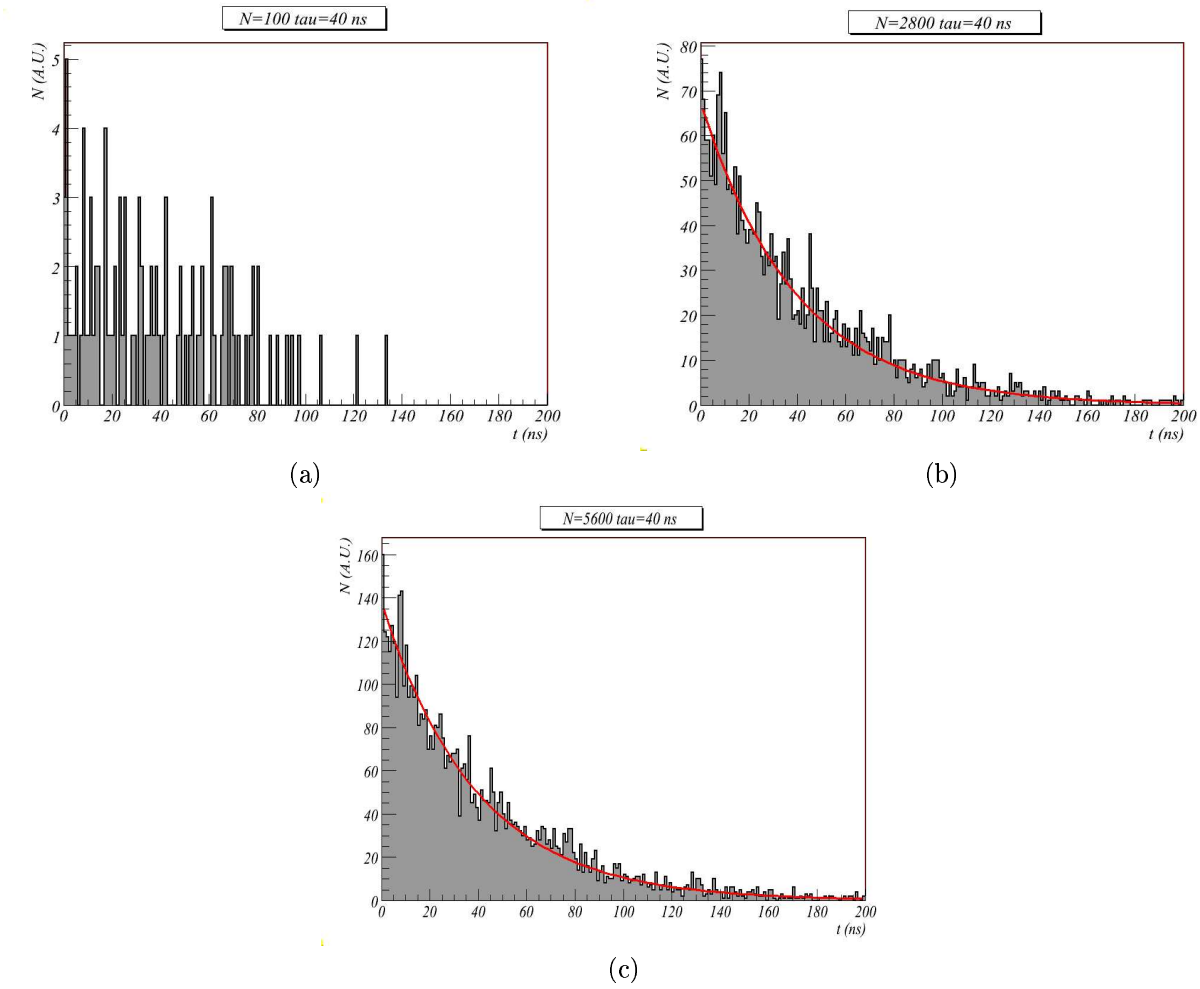

Figure 1: Distribution of the emission time from the generation of N photoelectrons according to the law $f(t) = \lambda\, exp(-\lambda t)$ with $\lambda = 40$ns (scintillation decay constant of LYSO) and constant $N = 100$ (a), $N = 2800$ (b), $N = 5600$ (c). The red line represents the $f(t)$ function.

The limits of $f(t)$ function are:

- $F(0) = 0$, implying that no light is emitted for $t < 0$
- $F(\infty) = 1$, which is the total emission probability of each photon

The probability distribution for the arrival time of the 1^{st} photoelectron among a total of N emitted photoelectrons is

$$p_1(t/N) = N\, F(t)\, [1 - F(t)]^{N-1} \tag{3}$$

The probability distribution for the arrival time of the k^{th} photoelectron among a total of N emitted photoelectrons is

$$p_k(t/N) = \frac{N!}{(k-1)!(N-k)!} [1 - F(t)]^{N-k}\, [F(t)]^{k-1}\, F(t) \tag{4}$$

The final probability distributions are obtained by the substitution of expressions (1) and (2) in (3) and (4),

$$p_1(t/N) = N\, \lambda\, e^{-\lambda t}\, [1 - 1 + e^{-\lambda t}]^{N-1} = N\, \lambda\, e^{-\lambda t}\, [e^{-\lambda t}]^{N-1} \tag{5}$$

$$p_k(t/N) = \frac{N!\,\lambda\,(1-e^{-\lambda t})^{k-1}}{(k-1)!\,(N-k)!}\,e^{-\lambda(N-k+1)} \tag{6}$$

2.1 Numerical application

2.1.1 Generic study

Figure 2 shows the arrival time probability distribution for 1^{st}, 10^{th}, 20^{th}, 50^{th} photoelectron according to expressions (5) and (6) for $p_1(t/N)$ and $p_k(t/N)$, respectively, with $\tau = 40ns$ (LYSO time constant).

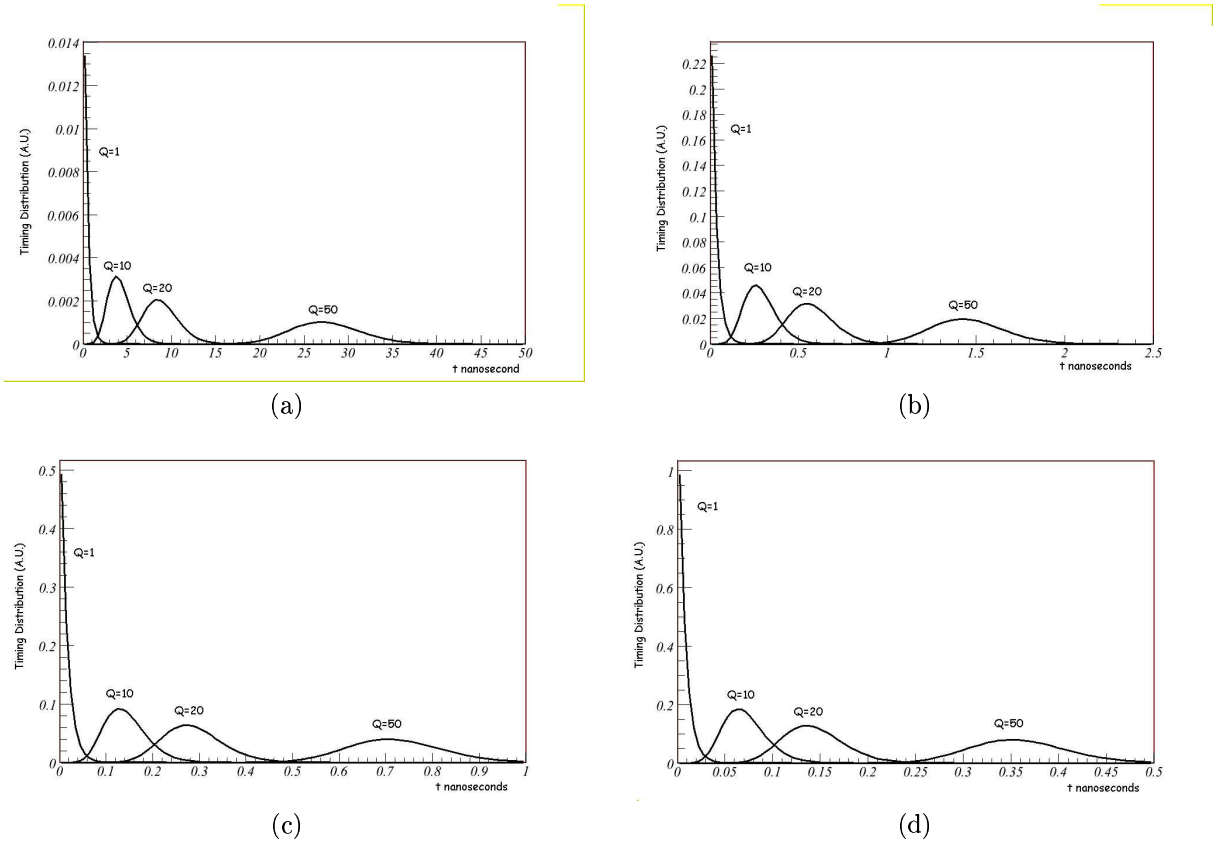

Figure 2: Arrival time probability distribution for 1^{st}, 10^{th}, 20^{th} and 50^{th} photoelectron of N photoelectrons with constant N equal to 100 (a), 1400 (b), 2800 (c) and 5600 (d), respectively.

To confirm these results, we simulate batches of 2000 events with N generated photoelectrons from scintillating law (1) and N fixed to 100, 1400, 2800 and 5600. For each batch, we plot the arrival time probability distribution of the 1^{st}, 10^{th}, 20^{th} and 50^{th} photoelectron. Figure 3 presents resulting distributions for N=2800 photoelectrons: these distributions confirm previous data. Similar distributions could be determined with batch of 2000 events of N photoelectrons with N distributed according to a Poisson law with $fwhm$ equal to 10% of the mean, N_m fixed to 100, 1400, 2800 and 5600.

All these results obtained by simulation are shown in Figure 4 for constant $N = 100$, 1400, 2800 and 5600, and for a Poisson distribution of N with fwhm equal to 10% of the mean, N_m, fixed to 100, 1400, 2800 and 5600.

The results confirm the decrease of arrival time dispersion for the k^{th} photoelectron when the number N of photoelectrons increase and when the order index k decreases.

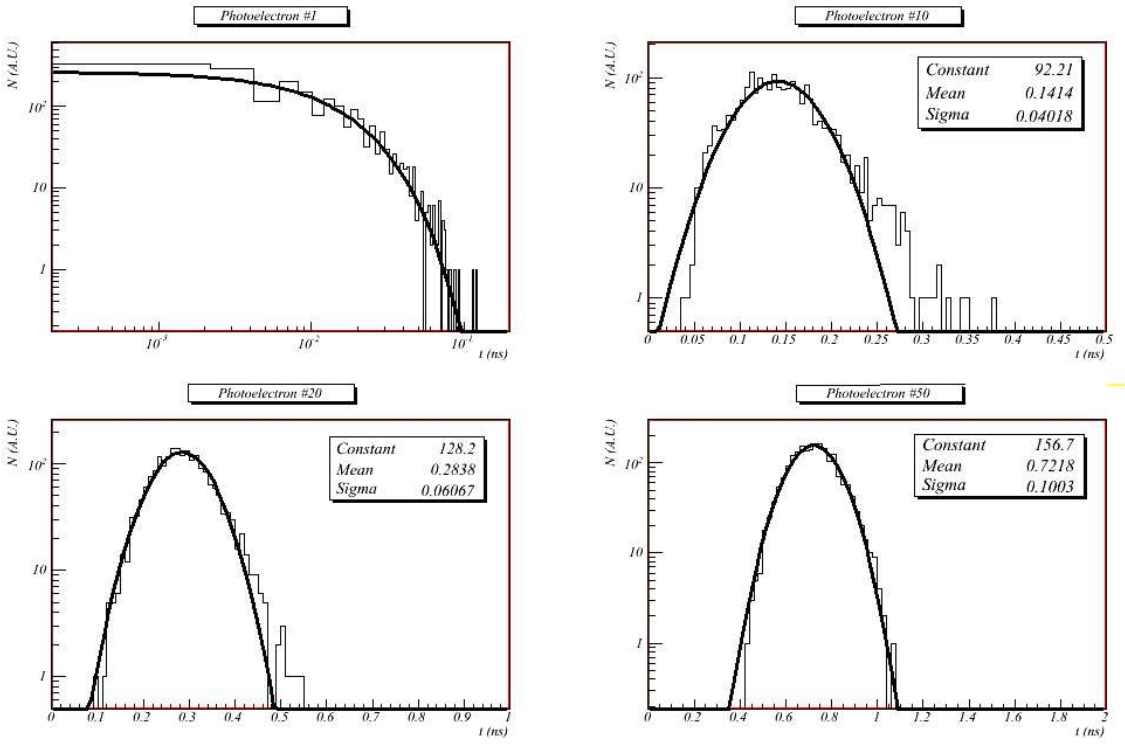

Figure 3: Arrival time distribution for 1^{st}, 10^{th}, 20^{th} and 50^{th} photoelectron for N generated photoelectrons from equation (1) with constant N=2800.

There is no significant difference between results of constant and variable values of N. If the mean number of photoelectrons is 2800 (LYSO crystal), we obtain the following results:

- the mean arrival time of the first photoelectron is 13.6ps with a standard deviation is 14.5ps
- the mean arrival time of the 10^{th} photoelectron is 140ps with a the standard deviation is 40ps

All numerical values are given in Appendix A.

Figure 5 represents the variance estimate of the k^{th} photoelectron arrival time distribution as a function of k, by using an analytical expression derived from Post and Schiff [POST50]:

$$\sigma^2(k) = \frac{k}{N^2\lambda^2}(1 + 2(1+k)/N + \dots) \tag{7}$$

All these results clearly show that the number of photoelectron in the event should be at least of the order of 1000 to perform accurate time of flight measurements. The increase of dispersion with the order number k is faster between 1 and 10 than between 10 and 20. It seems necessary to trigger on a photon whose order number is less than 10 to get a proper time resolution.

2.1.2 Comparison of LYSO and $LaBr_3$ crystals

A second simulation is performed for comparing time distributions of successive photoelectrons of two crystals: Prelude^{TM} (LYSO) and Brillance^{TM} ($LaBr_3$) from St Gobain Crystals. Appendix D sums up the main features of several crystals.

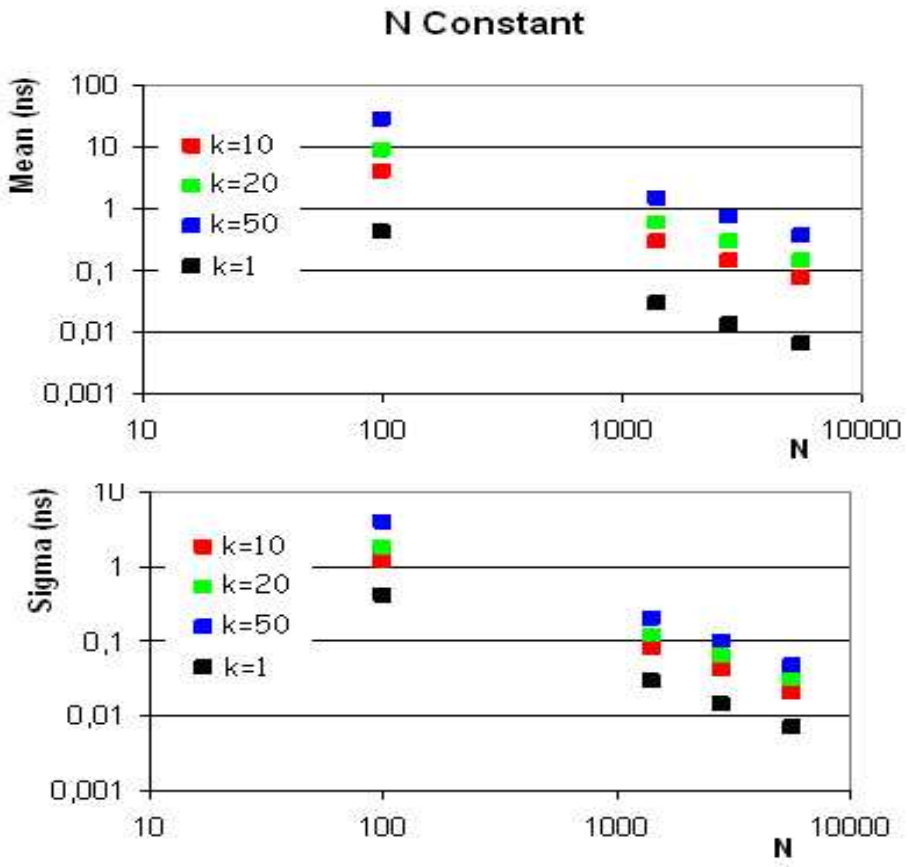

Figure 4: Mean time (top) and standard deviation (bottom) of the k^{th} photoelectron arrival time distribution, as a function of the number N of generated photoelectrons in the event. N is constant for each event and equal to 100, 1400, 2800 and 5600.

The $LaBr_3$ shows better characteristics than LYSO: on the one hand, its light yield is twice that of the LSO, and on the other hand, the scintillation decay constant of $LaBr_3$ is 16ns, compared to 40ns for LYSO.

The number N of photoelectrons is kept constant in each event. For LYSO, $N = 2800$ photoelectrons and $\tau = 40ns$. For $LaBr_3$, $N = 5600$ and $\tau = 16ns$. In both cases, 10000 events are generated.

For each event, N arrival times are randomly generated according to expression (1) and these times are sorted by increasing order. The mean and variance of the arrival times of the k^{th} photoelectron are finally calculated from the set of events.

We show in Figure 8, 9 and 10, the mean and the variance of the arrival time of the k^{th} photoelectron as a function of k.

We notice a linear variation of the mean arrival time as a function of the order index k.

The standard deviation of the arrival time of the k^{th} photoelectron increases as $\sqrt{k}$, in accordance with eq. (7) for k/N small.

Fig. 10 illustrates the initial increase of the arrival time spread of successive photoelectrons as $\sqrt{< t >}$. The dispersion of the first arrival times is very low (about some 10ps) and increases rapidly with the order index of the detected photoelectron, and thus with

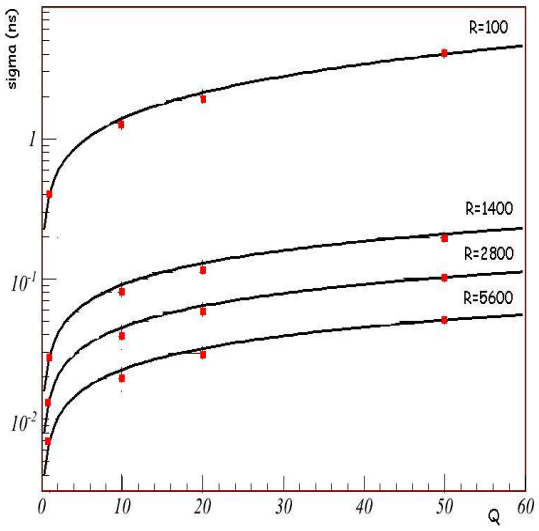

Figure 5: Variance of the k^{th} photoelectron arrival time as a function of N and k, according to the Post and Schiff expression [POST50]

its mean arrival time. The standard deviation is 150ps (500ps fwhm in coincidence) for the 106^{th} photoelectron, corresponding to a mean arrival time of 1.54 ns. The results are presented in Appendix C.

2.2 Extension to high values of the order index k

2.2.1 Photoelectrons of high order index and dispersion of the barycenter

If the triggering is based on a digital method implying the full signal, the measured time is affected by late photoelectrons. The arrival times of these late photoelectrons are much more dispersed than those of the first ones.

When the signal is shaped with a large time constant, the fluctuations of the signal are smoothened and the arrival time of the signal should be correlated to the barycenter of the PMT pulse. This barycenter is the mean arrival time of the contributions of each photoelectron to the pulse. The mean is weighed by the charge of the PMT response to individual photoelectrons.

$$T_m = \frac{\int_0^\infty ts(t)dt}{\int_0^\infty s(t)dt} = \frac{\sum_{i=1}^N t_i q_i}{\sum_{i=1}^N q_i} \tag{8}$$

If the photomultiplication process is supposed reproducible, producing the same output charge for each primary photoelectron ($\sigma_q = 0$), then

$$T_m = \frac{1}{N}\sum_i t_i \tag{9}$$

The variance of this mean time is given by:

$$var(T_m) = \frac{\tau^2}{N} \tag{10}$$

For LYSO crystal, ($\tau = 40$ns and $N = 2800$), we find a standard deviation of 730ps on the barycenter Tm, implying 2.4ns fwhm in coincidence. If the dispersion of the PMT

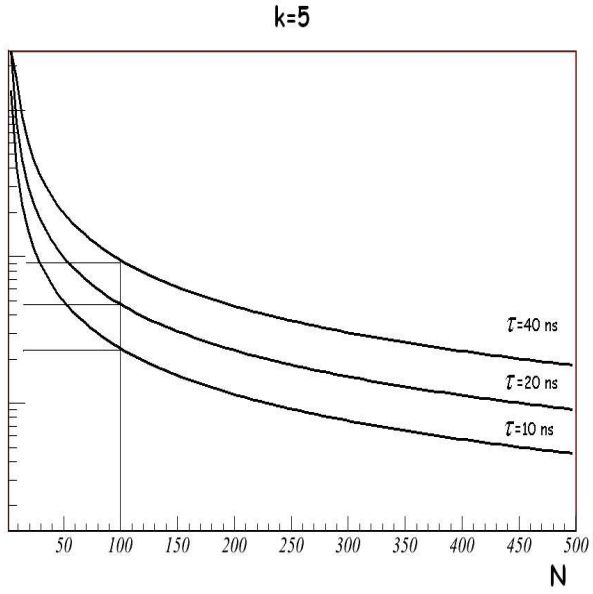

Figure 6: Variance as function of τ and N, according to the Post and Schiff expression, for $k = 5$
- $N = 100$ and $\tau = 40ns$, $\sigma = 0.9ns$
- $N = 100$ and $\tau = 20ns$, $\sigma = 0.45ns$
- $N = 100$ and $\tau = 10ns$, $\sigma = 0.22ns$

response charges q_i is taken into account, the simulation gives a standard deviation of 775ps, or 2.6ns fwhm in coincidence.

This raises the problem for time measurement methods based on the integral of the signal.

2.2.2 Elimination of late photoelectrons

If the photoelectrons arriving after a time threshold t_c are eliminated, the dispersion of the mean time T_m increases with t_c according to the behavior illustrated in Figure 11 for a LYSO crystal.

The standard deviation is 150ps (or 500ps fwhm in coincidence) for $t_c = 17$ns. This confirms the importance of triggering on the first photoelectrons for a good time resolution.

2.3 Conclusion

For k/N small, the standard deviation of the arrival times of the k_{th} photoelectron is close to $\sqrt{k}\,\tau/N$ (see eq. (7)).

The dispersion of the arrival time of the first photoelectrons is very low and increases rapidly with the order index, and hence with the arrival time of the detected photoelectrons.

The analog time pick-up technique based on constant fraction discriminator benefits from all these properties. The triggering is determined by the initial rapidly rising edge of the signal and ignores the late photoelectrons, whose times are more dispersed. This analog technique is currently the best to obtain good time resolutions.

In a time measurement technique based on the detection of the k^{th} photoelectron, the dispersion of time increases with the order index k of the photoelectron.

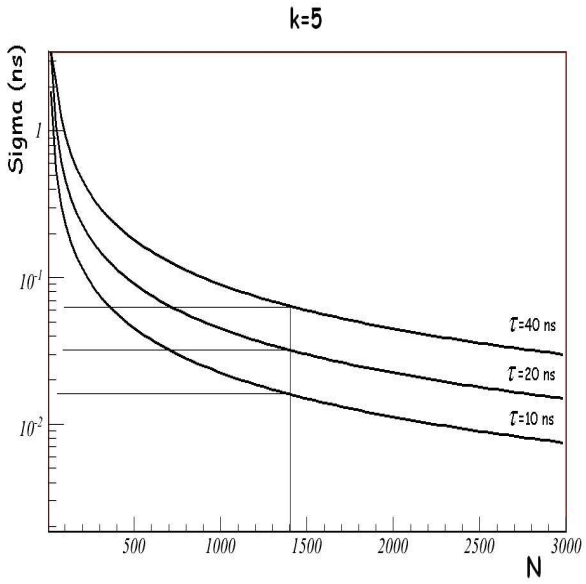

Figure 7: Variance as function of τ and N, according to the Post and Schiff expression, for $k = 5$
- $N = 1400$ and $\tau = 40ns$, $\sigma = 0.065ns$
- $N = 1400$ and $\tau = 20ns$, $\sigma = 0.032ns$
- $N = 1400$ and $\tau = 10ns$, $\sigma = 0.016ns$

The better is crystal light yield, the lowest will be the dispersion of the arrival time of the k^{th} photoelectron.

The scintillation time constant of the crystal is also an important factor for the resolution of this time measurement method.

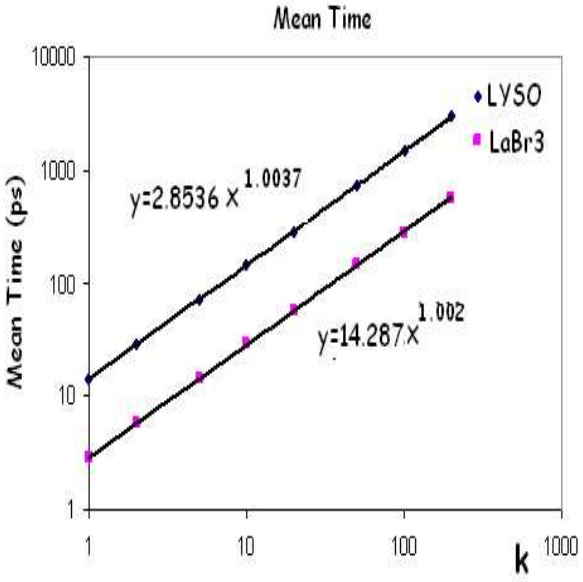

Figure 8: Mean arrival time of the k^{th} photoelectron as a function of the order of the detected photoelectron k (log-log scales), in the cases of LYSO and $LaBr_3$ crystals. The simulation parameters are $N = 2800$ and $\tau = 40$ ns for the LYSO crystal and $N = 5600$ and $\tau = 16$ ns for the $LaBr_3$ crystal.

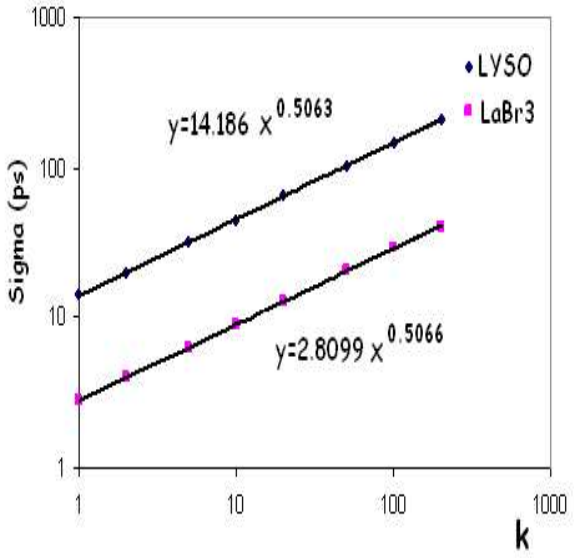

Figure 9: Standard deviation of the arrival time as a function of the order index k of the photoelectron considered, for LYSO and $LaBr_3$ crystals. The simulation parameters are $N = 2800$ and $\tau = 40$ ns for the LYSO crystal and $N = 5600$ and $\tau = 16$ ns for the $LaBr_3$ crystal.

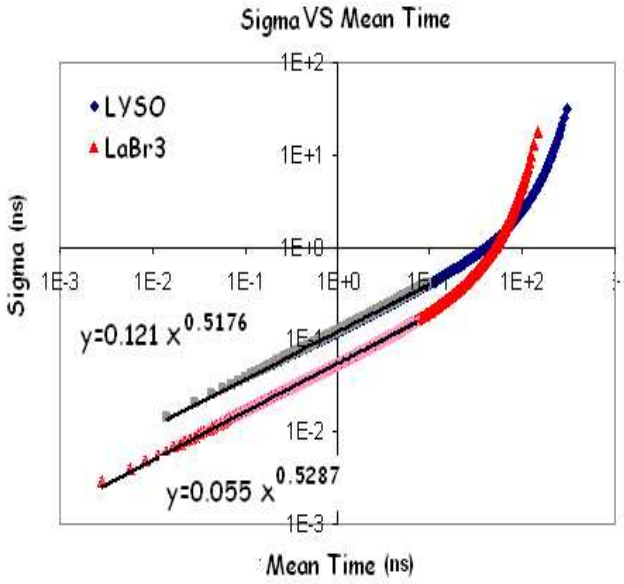

Figure 10: Correlation between the mean arrival time (x axis) and the dispersion (y axis) of the distribution of arrival time of the k^{th} photoelectron for LYSO and $LaBr_3$ crystals. The simulation parameters are $N = 2800$ and $\tau = 40$ ns for the LYSO crystal and $N = 5600$ and $\tau = 16$ ns for the $LaBr_3$ crystal.

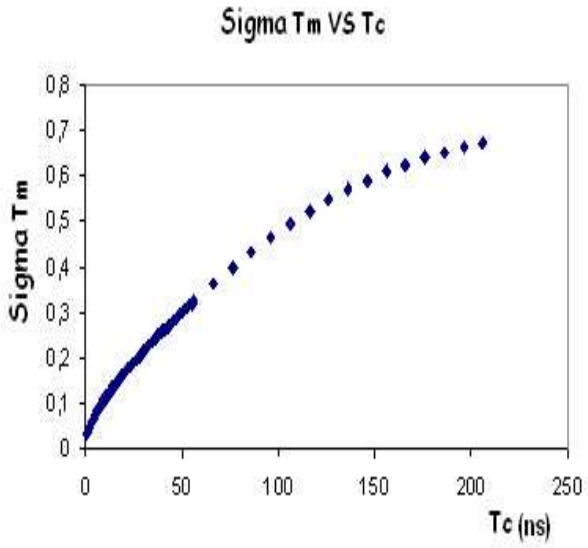

Figure 11: Dispersion of the barycenter as a function of the cut time: $\tau = 40$ns and $N = 2800$.

3 Optimal filtering

The optimal filtering method is currently used in high energy physics experiments, especially LHC experiments (ATLAS, CMS). Most recent results concern calorimetry of such experiments [FULL05]. This method is used for the estimation of energy and time from digital samples of the measured signal. The algorithm requires the preliminary determination of two sets of coefficients from samples of the signal. During the acquisition, time and energy are reconstructed by two sums of the signal samples weighed by the coefficients. The optimal filtering method is presented in Appendix F.

3.1 Constant number of photoelectrons

To implement the optimal filtering method:

- a reference mean signal (amplitude-normalized) is calculated and coefficients are determined
- batches of 2000 events are simulated and the times are reconstructed

Batches of 2000 events are simulated with photoelectrons number N fixed to 100, 1400, 2800. The arrival times of the N photoelectrons $(t_1, t_2 \ldots, t_N)$ are generated according to the scintillation law (1), digitized with a 0.1ns bin and sorted by increasing time.

Each photoelectron contributes to the global pulse according to the response function of the $CR - RC^2$ shaper to a Dirac current pulse.

$$f(x) = \left(\frac{x^2}{2} - \frac{x^3}{6}\right) exp(-x) \tag{11}$$

In this expression $x = (t - t_i)/\lambda$, t being the current time of the event, t_i the emission time of the considered photoelectron, and λ the time constant common to the preamplifier and the shaper. This parameter is set to $150ns$, $50ns$, $20ns$.

Figure 12 shows the responses of $CR-RC$ and $CR-RC^2$ shapers with time constants 150ns, 50ns, 20ns to a Dirac pulse.

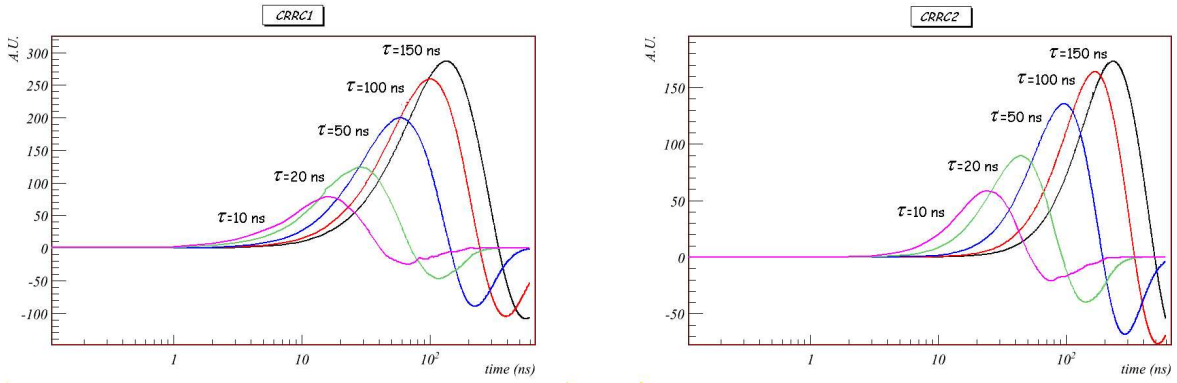

(a) (b)

Figure 12: Responses of $CR - RC$ (a) and $CR - RC^2$ (b) shaping with time constants 150ns, 50ns, 20ns to a Dirac current pulse.

We choose a $CR - RC^2$ shaping (with time constant 150ns, 50ns, 20ns) and set the sampling frequency to 50MHz, 100MHz, 200MHz and 1GHz.

Figure 13 summarizes the time resolutions after optimal filtering at 50MHz and 1GHz sampling frequency. The results for all frequencies tested are tabulated in appendix (B).

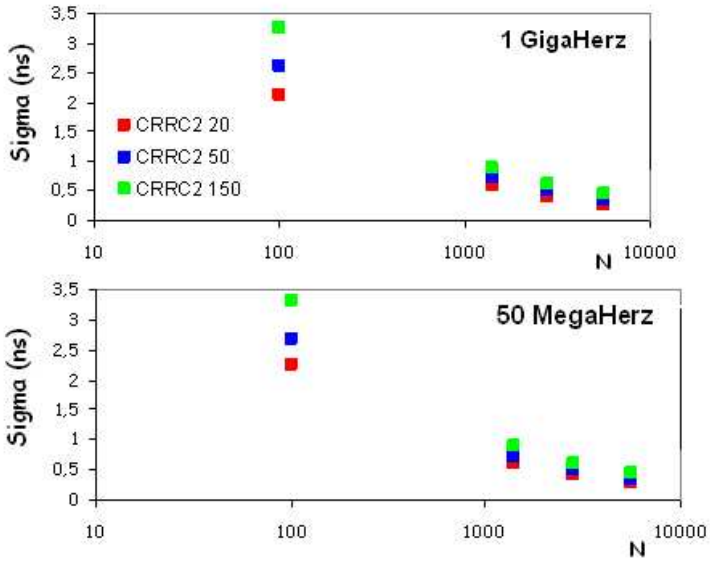

Figure 13: Time resolutions of optimal filtering reconstruction, for 50MHz and 1GHz sampling frequency, as a function of the time constant of a $CR - RC^2$ shaper, and as a function of the number N of photoelectrons per event.

Time resolution improves when the shaping time is short and the number of photoelectrons high and clearly demonstrate that results do not differ significantly with sampling frequencies.

3.2 Variable number of photoelectrons

First, a reference signal with low statistical fluctuation is constructed from a large number of generated photoelectrons(100,000) generated according to the scintillation law (1). The reference samples, the time at the signal maximum and the coefficients are calculated from the reference signal.

Then, a batch of 10,000 events is generated

- The number N of photoelectrons in the event is generated according to a normal law centered on N_0 and with standard deviation σ_n determined by the crystal resolution R_c: $\sigma_n = N_0\, R_c/2.35$; $R_c = 10\%$
- The arrival times t_i ($i = 1$ to N) of each photoelectrons are generated according to the scintillation law (1)
- The final signal is shaped and sampled at the frequency F, and the amplitude and time at the maximum are estimated by optimal filtering

In this configuration with variable number of photoelectrons, we study the influence of two parameters: the mean number of event photoelectrons and the sampling frequency. The shaper is a $CR-RC$ circuit, with a 20ns time constant. The considered scintillator decay time is 40ns (LYSO).

3.2.1 Effect of the mean number of photoelectrons

The simulations are implemented with $N_0 = 100$, 1400, 2800, 5600, 11200 photoelectrons. Figure 14 shows the coincident time resolution as a function of the mean number of

photoelectron.

The dispersions are expressed in standard deviation (sigma) and full width at half the maximum in coincidence. The relation between fwhm and sigma for a Gaussian distribution is

$$fwhm = 2\sqrt{2ln2} \approx 2.35\sigma \tag{12}$$

In coincidence, we add the errors in quadrature:

$$fwhm_{coinc} = 2\sqrt{2}\sqrt{2ln2} \cdot \sigma \approx 3.33\sigma \tag{13}$$

CRRC	shaping 20ns		
100MHz (10ns) sampling			
N	sigma_t (ns)	fwhm_coinc (ns)	ampli resol
100	2,076	6,914	7,9%
1400	0,580	1,931	2,3%
2800	0,401	1,335	1,8%
5600	0,283	0,941	1,6%
11200	0,226	0,754	1,5%

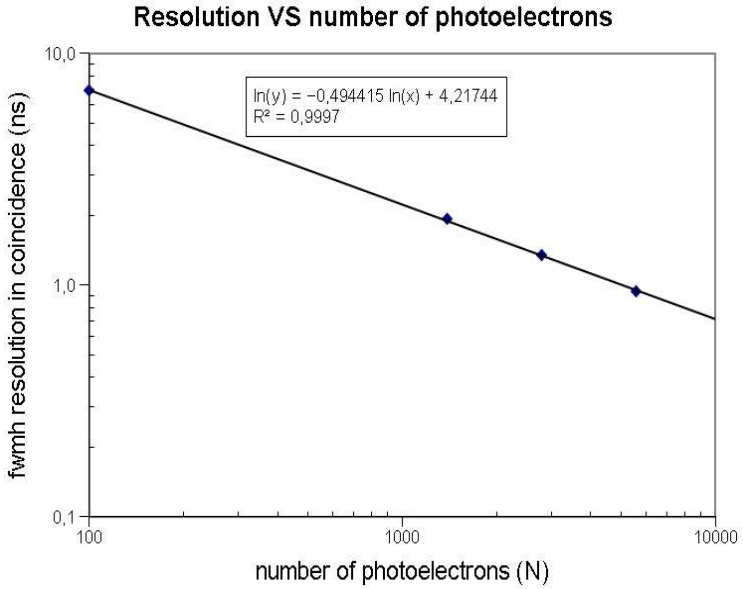

Figure 14: Resolution (fwhm in coincidence) of the times reconstructed by optimal filtering for $N =$ 100, 1400, 2800, 5600, 11200. The shaping is a $CR - RC$ circuit with a 20ns time constant and the sampling frequency is 100MHz.

We can see that the dispersion of reconstructed times scales as $\tau/\sqrt{N}$. This trend is similar to that observed for the dispersion of the signal's barycenter (see section 1.2.a). Indeed, as for the time at the barycenter of the signal, the time reconstructed by optimal filtering is sensitive to all photoelectrons (or the large number of those which contribute to the positive lobe of the shaped signal).

3.2.2 Effect of sampling frequency

The simulations are performed with sampling frequencies $F = 50$MHz, 200MHz, 500MHz. Figure 15 shows the coincident time resolution as a function of the sampling frequencies.

The resolution does not depend significantly on sampling frequency above F=100MHz. This result indicates that the number of samples describing the pulse is not the limiting factor for this time reconstruction method.

CRRC	shaping 20ns		
N=2800 photoelectrons			
F (MHz)	sigma_t (ns)	fwhm_coinc (ns)	ampli resol
50	0,467	1,557	4,7%
100	0,401	1,335	1,8%
200	0,384	1,278	1,5%
500	0,393	1,310	1,5%

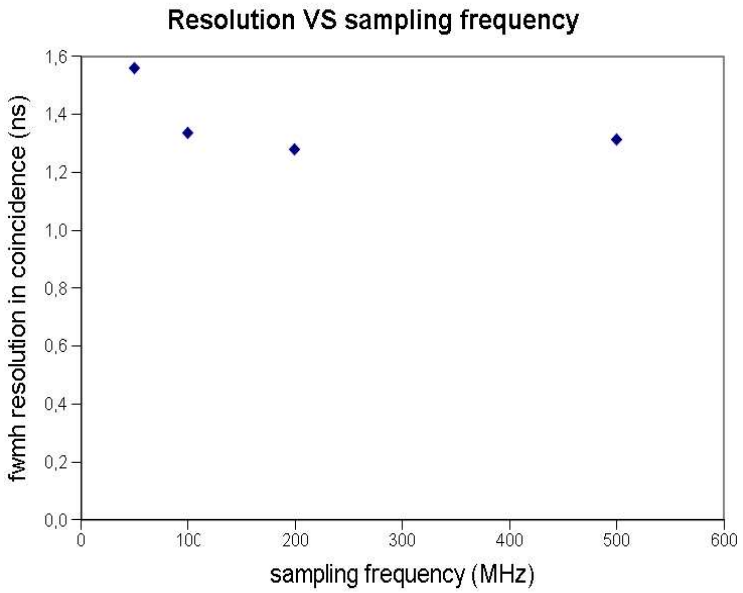

Figure 15: Resolution (fwhm in coincidence) on times reconstructed by optimal filtering for $F = 50$MHz, 200MHz, 500MHz. The number of photoelectrons N of the event is 2800. The shaping is a $CR - RC$ circuit with a 20ns time constant.

3.3 Effect of shaping

3.3.1 Sampling frequency: 100MHz

The sampling frequency is set to 100MHz and the number of photoelectrons is 2800. The scintillation time constant is still 40ns. Simulations are performed with shaping time constants adjusted for peaking time to be 20ns, 50ns, 100ns and 150ns. Figure 16 shows the coincident time resolution for $CR-RC$ and $CR-RC^2$ shaping with different peaking time.

We notice that resolution improves when peaking time decreases, until a certain optimum.

We propose the following interpretation: the duration T_+ of the positive lobe, which is the only part of the signal processed by optimal filtering, increases with shaping time. Consequently, the photoelectrons arriving with a delay larger than T_+ after the first one do not influence the reconstructed time. So that the duration of the positive lobe acts as a cut time (Cf 1.2.b).

For very short peaking times, the resolution degrades because the number of samples in the rising edge becomes insufficient.

3.3.2 Sampling frequency: 200MHz

Now, the sampling frequency is set to 200MHz and the number of photoelectrons is 2800. The scintillation time constant is still 40ns. Simulations are performed with shaping time constants adjusted for peaking time to be 20ns, 50ns, 100ns and 150ns. Figure 17 shows

CR-RC	100MHz (10ns) sampling		2800 photoelectrons	
Tshaping (ns)	Peaking t (ns)	sigma t (ns)	fwhm coinc (ns)	ampli resol
12,3	20	0,488	1,624	3,4%
40,0	51	0,460	1,531	1,2%
102,6	101	0,568	1,892	0,7%
168,4	144	0,606	2,017	0,6%

CR-RC²	100MHz (10ns) sampling		2800 photoelectrons	
Tshaping (ns)	Peaking t (ns)	sigma t (ns)	fwhm coinc (ns)	ampli resol
8,0	21	0,370	1,232	4,1%
22,9	51	0,442	1,472	1,5%
52,9	100	0,546	1,818	0,8%
90,7	154	0,643	2,141	0,7%

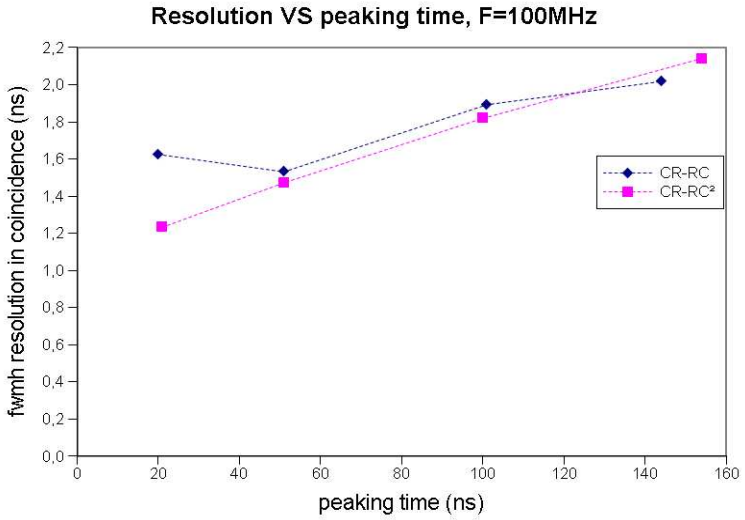

Figure 16: Resolution (fwhm in coincidence) on the times reconstructed by optimal filtering for a $CR-RC$ and $CR-RC^2$ shaping with 20, 50, 100, 150ns peaking time. The sampling frequency is 100MHZ and the number N of photoelectrons in the event is 2800.

the coincident time resolution in such conditions and indicates that

resolution improves when peaking time decreases. The optimum shaping found in the previous behavior (for F=100MHz) does not appear here. It probably exists at lower shaping time, as the sampling step is divided by 2.

3.4 Conclusion

The time resolution of optimal filtering scales as $\tau/\sqrt{N}$ and increases with the shaping time λ. The amplitude resolution, on the contrary, improves when λ increases, and is always good with respect to the crystal energy resolution (10%).

The $CR-RC^2$ shaping leads to a slightly better time resolution than $CR-RC$, if the results are compared for equal peaking time.

The effect of sampling frequency is weak, especially beyond 100MHz. This is due to the limitation of time resolution imposed by the dispersion of arrival time of photoelectrons with high order number.

Both series of simulations (constant N and Gaussian distributed N) give equivalent results.

CR-RC	200MHz (5ns) sampling		2800 photoelectrons	
Tshaping (ns)	Peaking t (ns)	sigma_t (ns)	fwhm_coinc (ns)	ampli resol
12,3	20	0,343	1,144	2,1%
40,0	51	0,476	1,585	1,0%
102,6	101	0,588	1,958	0,7%
168,4	144	0,614	2,044	0,6%

CR-RC2	200MHz (5ns) sampling		2800 photoelectrons	
Tshaping (ns)	Peaking t (ns)	sigma_t (ns)	fwhm_coinc (ns)	ampli resol
8,0	21	0,323	1,075	2,2%
22,9	51	0,438	1,459	1,2%
52,9	100	0,552	1,840	0,8%
90,7	154	0,618	2,059	0,6%

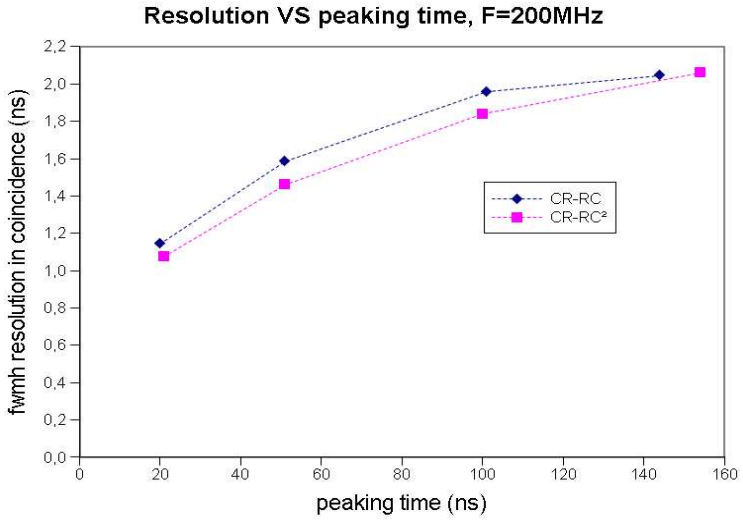

Figure 17: Resolution (fwhm in coincidence) on the times reconstructed by optimal filtering for a $CR-RC$ and $CR-RC^2$ shaping with 20, 50, 100, 150ns peaking time. The sampling frequency is 200MHZ and the number N of photoelectrons in the event is 2800.

For LYSO crystal: $N = 2800$phe, $\tau = 40$ns, with 100MHz sampling frequency and 50ns peaking time, we estimate a fwhm time resolution in coincidence equal to

- 1.53ns for a $CR-RC$ circuit, N variable (table 1 section 3.3.2)
- 1.47ns for a $CR-RC^2$ circuit, N variable (table 2 section 3.3.2)

For $LaBr_3$ crystal: $N = 5600$phe, $\tau = 16$ns, with 100MHz sampling frequency and 50ns peaking time, we extrapolate the results obtained for LYSO (as time resolution scales as $\tau/\sqrt{N}$):

- 0.43ns for a $CR-RC$ circuit, N variable (table 2.3)
- 0.41ns for a $CR-RC^2$ circuit, N variable (table 2.3)

4 Variable fraction discriminator (VFD)

We will now investigate a numerical method inspired by constant fraction discriminator, and applied to a sampled signal. The time is extracted from samples on the rising edge of the signal. Contrary to the CFD electronics, which picks-up the time when the signal reaches a constant fraction of the maximum, the VFD algorithm performs a time correction corresponding to a measured fraction: the ratio of the first sample to the amplitude. This measured ratio is variable, hence the name of this algorithm.

4.1 Principle of the VFD algorithm

From the reference signal normalized by the maximum, we build a "look-up table" describing the rising edge of the signal: for successive values x_i of normalized signal, the corresponding times $t(x_i)$ are recorded in the "look-up table".

When the events are analyzed, the first sample s_i greater than a fixed threshold triggers the process. The fraction $X = s_i/max$ is calculated, and if x is greater than 5%, time is calculated in a two-step process.

First, the "look-up table" is read at the address corresponding to a rounded value of x, and the two time values surrounding $t(x)$ are read. Then, the precise time t of the signal is calculated by linear interpolation. Figure 18 shows the implementation of the VFD algorithm.

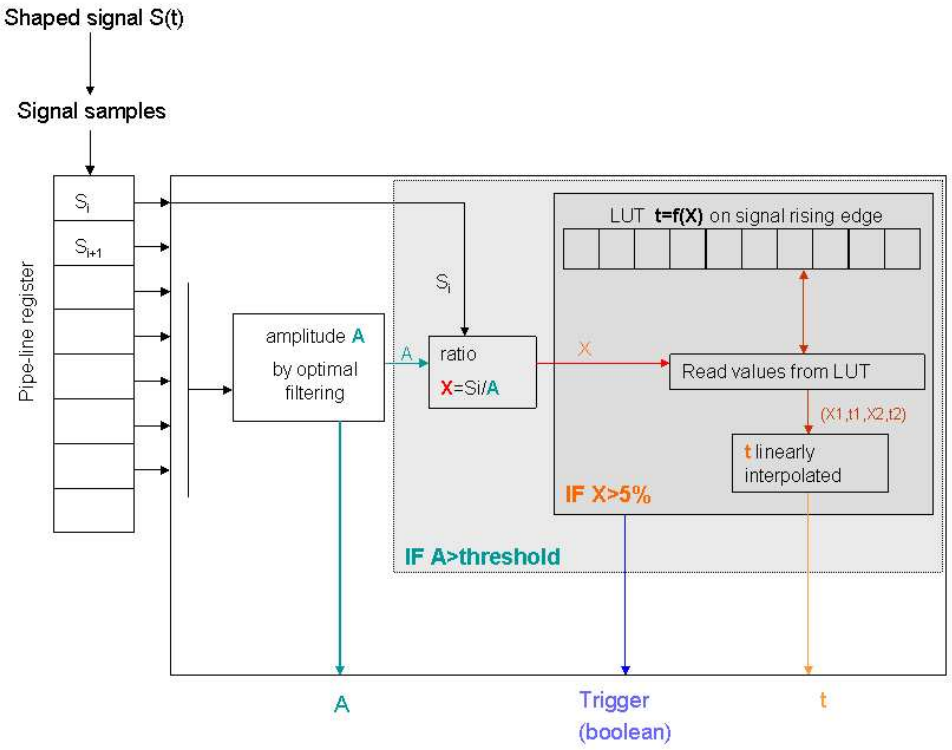

Figure 18: Logical schematics of the VFD algorihm implementation

4.2 Results

The previous analysis were repeated with the VFD method. The results are compared to standard optimal filtering method.

4.2.1 Effect of the number of photoelectrons

Figure 19 represents the comparison of coincident time resolution either by optimal filtering or by VFD method, as a function of the number of photoelectrons $N = 100$, 1400, 2800, 5600, 11200. The $CR-RC$ shaping time constant is 20ns and the sampling frequency 100Mhz. The time resolution of the VFD method appears better than optimal filtering for all values of N. The dispersion of reconstructed times scales as $\tau/\sqrt{N}$ for both methods.

	CRRC	shaping 20ns			
		100MHz (10ns) sampling			
	VFD		optimal filtering		
N	sigma_t (ns)	fwhm_coinc (ns)	sigma_t (ns)	fwhm_coinc (ns)	ampli resol
100	1,249	4,158	2,076	6,914	7,9%
1400	0,322	1,071	0,580	1,931	2,3%
2800	0,226	0,753	0,401	1,335	1,8%
5600	0,160	0,532	0,283	0,941	1,6%
11200	0,131	0,436	0,226	0,754	1,5%

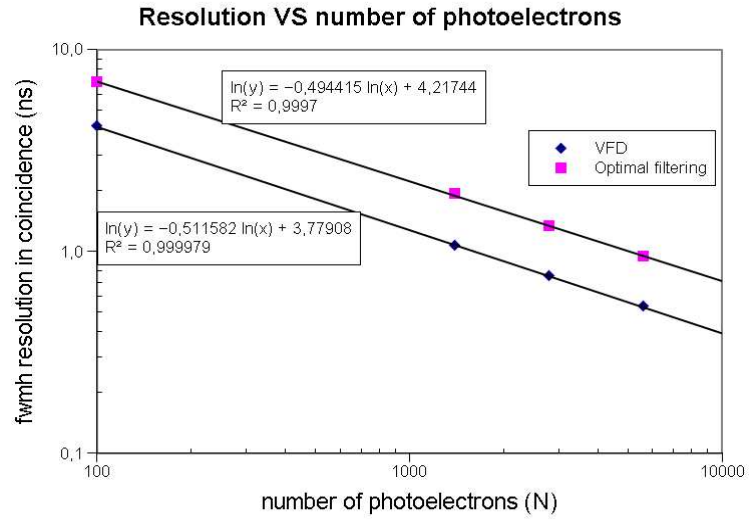

Figure 19: Comparison of time resolution in coincidence obtained either by optimal filtering or by VFD method, as a function of the number of photoelectrons $N = 100$, 1400, 2800, 5600, 11200. The $CR-RC$ shaping time constant is 20ns and the sampling frequency 100Mhz.

4.2.2 Effect of sampling frequency

Figure 20 represents the comparison of coincident time resolution either by optimal filtering or by VFD method, as a function of the sampling frequency $F = 50$MHz, 100MHz, 200MHz, 500MHz. The number of photoelectrons is $N = 2800$ and the $CR-RC$ shaping time constant is 20ns.

The VFD timing resolution improves with sampling frequency, while the optimal filtering timing resolution remains almost constant. Indeed, as the sampling frequency increases, the first sample gets closer to the beginning of the signal and the photons involved in the time measurements are only the first ones.

CRRC	shaping 20ns		2800 photoelectrons		
	VFD		optimal filtering		
F (MHz)	sigma_t (ns)	fwhm_coinc (ns)	sigma_t (ns)	fwhm_coinc (ns)	ampli resol
50	0,364	1,211	0,467	1,557	4,7%
100	0,226	0,753	0,401	1,335	1,8%
200	0,165	0,549	0,384	1,278	1,5%
500	0,129	0,429	0,393	1,310	1,5%

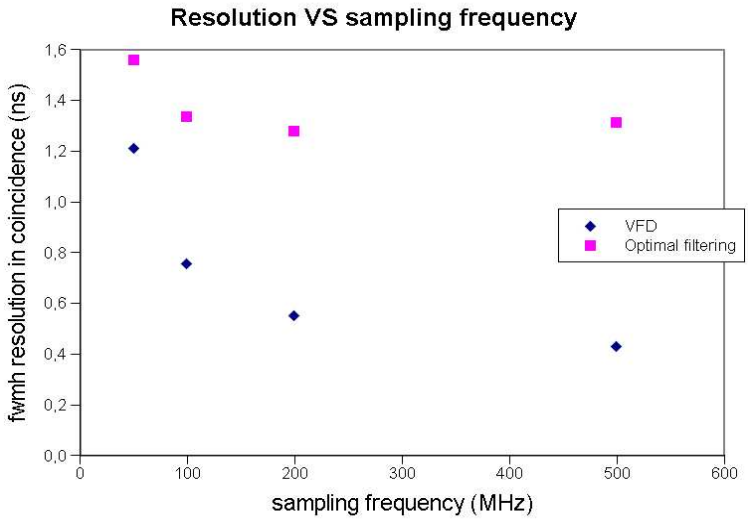

Figure 20: Comparison of time resolution in coincidence obtained either by optimal filtering or by VFD method, as a function of the sampling frequency $F = 50$MHz, 100MHz, 200MHz, 500MHz. The number of photoelectrons is $N = 2800$ and the $CR - RC$ shaping time constant is 20ns.

4.2.3 Effect of shaping

The number of photoelectrons is $N = 2800$ and the time constant is still 40ns. Simulations are performed for $F = 100$MHz (Figure 21) and 200MHz (Figure 22) with CR-RC and CR-RC^2 shaping, with time constants $\lambda = 10$ns, 20ns, 50ns, 100ns. Figure 21 represents the comparison of coincident time resolution either by optimal filtering or by VFD method, as a function of the shaping time constant: 10ns, 20ns, 50ns and 100ns for $CR - RC$ and $CR - RC^2$ shaping. The number of photoelectrons is $N = 2800$ and the sampling frequency is $F = 200$MHz. Figure 21 represents the same comparison for a sampling frequency $F = 100$MHz

4.3 Comparison with optimal filtering

The dispersion of times determined by the VFD algorithm are always smaller than those obtained by optimal filtering, with a gain factor close to 2.

The resolutions of both methods scale as $1/\sqrt{N}$, similarly to the dispersion of the signal barycenter (with a time cut).

The VFD resolution improves when sampling frequency increases and when shaping time decreases until an optimal value.

These results strengthen the importance of the beginning of the signal for time measurement.

We can estimate some time resolution limits for VFD (the results for optimal filtering are reminded in brackets):

	CR-RC	100MHz (10ns) sampling		2800 photoelectrons		
		VFD		filtrage opt		
Tshaping (ns)	Peaking t (ns)	sigma_t (ns)	fwhm_coinc (ns)	sigma_t (ns)	fwhm_coinc (ns)	ampli resol
12,3	20	0,251	0,837	0,488	1,624	3,4%
40,0	51	0,225	0,749	0,460	1,531	1,2%
102,6	101	0,245	0,816	0,568	1,892	0,7%
168,4	144	0,260	0,865	0,606	2,017	0,6%

	CR-RC2	100MHz (10ns) sampling		2800 photoelectrons		
		VFD		filtrage opt		
Tshaping (ns)	Peaking t (ns)	sigma_t (ns)	fwhm_coinc (ns)	sigma_t (ns)	fwhm_coinc (ns)	ampli resol
8,0	21	0,219	0,728	0,370	1,232	4,1%
22,9	51	0,205	0,684	0,442	1,472	1,5%
52,9	100	0,230	0,766	0,546	1,818	0,8%
90,7	154	0,260	0,866	0,643	2,141	0,7%

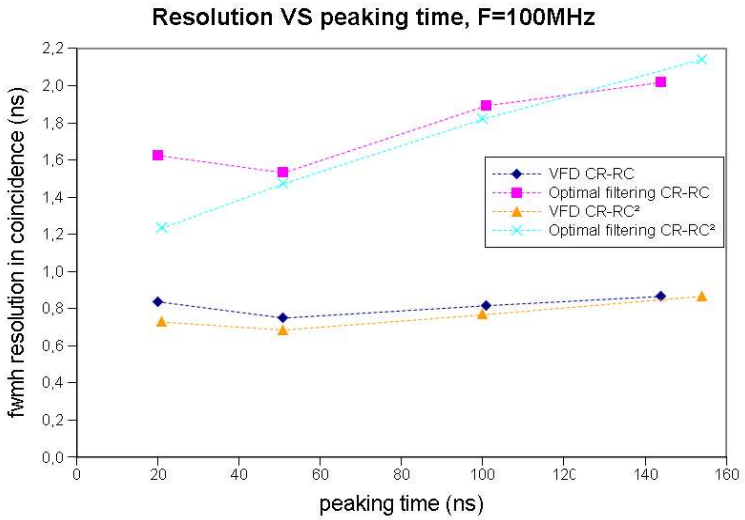

Figure 21: Comparison of time resolution in coincidence obtained either by optimal filtering or by the VFD method, as a function of shaping time constant = 10ns, 20ns, 50ns, 100ns for $CR-RC$ and CR-RC^2 shaping. The number of photoelectrons is $N = 2800$ and the sampling frequency 200MHz.

For a LYSO crystal: $N = 2800$phe, $\tau = 40$ns, with a 100MHz sampling and a shaping with $\lambda = 50$ns peaking time, we estimate a fwhm time resolution in coincidence of

- 0.75ns (1.53ns) in the case of $CR-RC$, N variable
- 0.68ns (1.47ns) in the case of $CR-RC^2$, N variable

For a $LaBr_3$ crystal: $N = 5600$phe, $\tau = 16$ns, with a 100MHz sampling and a 50ns peaking time, we evaluate the fwhm coincidence time resolution with the relation $\sigma\tau/\sqrt{N}$

- 0.21 (0.43) in the case of $CR-RC$, N variable
- 0.19 (0.41) in the case of $CR-RC^2$, N variable

Timing performances appear strongly dependent on

- The primary photoelectron yield of the detector (determined by the scintillator light yield, its geometry and surface finish, the optical coupling and the photodetector quantum efficiency)
- The scintillator decay constant
- The time reconstruction technique and configuration (signal shaping, sampling frequency, type of algorithm)

CRRC	200MHz (5ns) sampling			2800 photoelectrons	
	VFD		filtrage opt		
Peaking t (ns)	sigma t (ns)	fwhm coinc (ns)	sigma t (ns)	fwhm coinc (ns)	ampli resol
20	0,163	0,541	0,343	1,144	2,1%
51	0,180	0,600	0,476	1,585	1,0%
101	0,212	0,708	0,588	1,958	0,7%
144	0,235	0,783	0,614	2,044	0,6%

CRRC2	200MHz (5ns) sampling			2800 photoelectrons	
	VFD		filtrage opt		
Peaking t (ns)	sigma t (ns)	fwhm coinc (ns)	sigma t (ns)	fwhm coinc (ns)	ampli resol
21	0,148	0,494	0,323	1,075	2,2%
51	0,171	0,568	0,438	1,459	1,2%
100	0,207	0,691	0,552	1,840	0,8%
154	0,246	0,818	0,618	2,059	0,6%

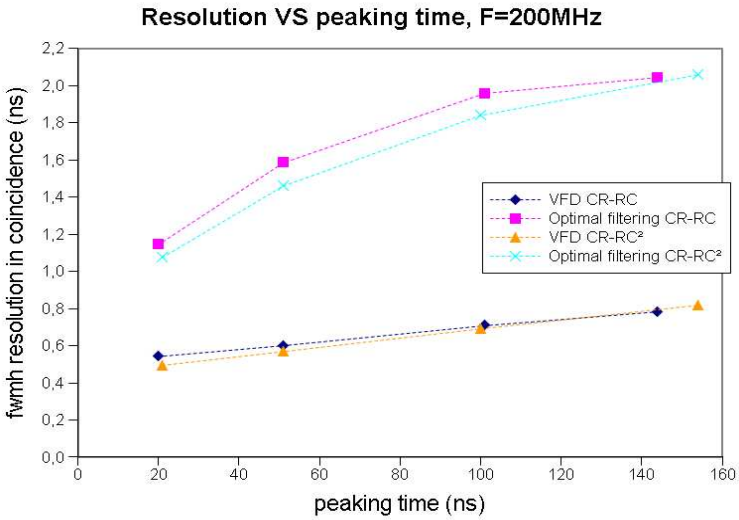

Figure 22: Comparison of time resolution in coincidence obtained either by optimal filtering or by the VFD method, as a function of shaping time constant = 10ns, 20ns, 50ns, 100ns for $CR - RC$ and $CR - RC^2$ shaping. The number of photoelectrons is $N = 2800$ and the sampling frequency 100MHz.

5 Discussion and perspectives

The preliminary results presented in this paper are useful for the intuitive comprehension of the limits of different methods for time measurements for TOF PET application.

In this study we have not taken into account the different factors that affect the crystal light output (e.g. photon traking in the crystal). LITRANI simulation code will be used for predicting the light attenuation for crystals with different geometries and wrappings [VILA06].

Present study will be also extended to other photodetectors such as APD and MCP-PMT.

References

[POST50] R.F. Post, L.I. Schiff, *Statistical limitations on the resolving time of a scintillation counter*, Phys.Rev., vol. 80, pp. 1113-1120, 1950

[KELB06] M. Kelbert, I. Sazonov, A.G. Wright, *Exact expression for the variance of the photon emission process in scintillation counters*, Nucl. Instr. and Meth., A 564, pp. 185-189, 2006

[RANU93] G. Ranucci, *Time statistics of the photoelectron emission process in scintillation counters*, Nucl. Instr. and Meth. Vol 335 (1-2), pp. 121-128, 1993

[WRIG99] A.G. Wright, *Fast timing with inorganic scintillators*, Electron Tubes ltd. Technical reprint R/P099

[HYMA65] L.G. Hyman, *Time resolution of photomultiplier tube systems*, Rev. Sci. Instr., Vol. 36, pp. 193-196, 1965

[MOSE06] W.W.Moses, *Factors Influencing Timing Resolution in a Commercial LSO PET Camera*, IEEE Trans. Nucl. Sci., Vol. 53, pp. 78-85, 2006

[MOSZ03] M.Moszynski et *al.*, *New Fast Photomultipliers with a Screening Grid at the Anode*, 2003 IEEE NSS Conference Record, vol. 2, pp. 1378-1383, 2003

[FALL01] A. Fallu-Labruyere, H. Tan, W. Hennig, and W.K. Warburton, *Time Resolution Studies using Digital Constant Fraction Discrimination*, Preprint Nuclear Instruments and Methods in Physics Research, 2006

[FULL05] E. Fullana et *al. Optimal Filtering in the ATLAS Hadronic Tile Calorimeter*, Atlas internal note ATL-TILECAL-2005-001, 2005

[VILA06] I. Vilardi et *al. Optimization of the effective light attenuation length of YAP: Ce and LYSO:Ce crystals for a novel geometrical PET concept*, Nucl. Instr. and Meth.A Vol 564, pp. 506-514, 2006

[OLCOTT06] P. D. Olcott et *al. A high speed fully digital data acquisition system for Positron Emission Tomography*, IEEE MIC proceedings, San Diego, 2006

[NIKOLIC04] I. Nikolic-Audit, L Serin *Time resolution of the ATLAS barrel liquid argon electromagnetic calorimeter*, ATl-LARG-002, janvier 2004

[SZCZ06] T. Szcześniak et *al. A Further Study of Timing with LSO on XP20D0 for TOF PET*, IEEE NSS MIC poster, San Diego, 2006

A Time characteristics of successive photoelectrons

Table of the mean (sigma) arrival time of the first, 10^{th}, 20^{th} and 50^{th} photoelectron for the events with constant $N = 100$, 1400, 2800 and 5600. The values are in picoseconds for the first photoelectron and in nanoseconds for higher index order results.

Mean(Sigma) of the 1st photoelectron (ps)		
	Constant N	Variable N
N=100	411 (410)	413(417)
N=1400	28(28.2)	27,7(27,9)
N=2800	13,6(14.5)	13,5(14,4)
N=5600	6,48(7)	6,47(7)

Mean (Sigma) of the 10th photolectron		
	Constant N	Variable N
N=100	4.11 (1.17)	4.14 (1.22)
N=1400	0.28 (0.078)	0.28 (0.08)
N=2800	0.14 (0.04)	0.143 (0.04)
N=5600	0.07 (0.02)	0.07 (0.02)

Mean (Sigma) of the 20th photoelectron		
	Constant N	Variable N
N=100	8.71 (1.85)	8.77 (1.9)
N=1400	0.57 (0.122)	0.57 (0.12)
N=2800	0.284 (0.06)	0.285 (0.06)
N=5600	0.142 (0.03)	0.141 (0.03)

Mean (Sigma) of the 50th photoelectron		
	Constant N	Variable N
N=100	27.3 (3.9)	27.65 (4.18)
N=1400	1.453 (0.2)	1.45 (0.206)
N=2800	0.722 (0.1)	0.72 (0.105)
N=5600	0.356 (0.047)	0.356 (0.049)

B Time resolution of optimal filtering, constant N

Table of optimal filtering time resolution for the events with N fixed to 100, 1400n 2800 and 5600. The shaping is $CR - RC^2$ with a 150ns, 50ns and 20ns time constant. The sampling frequency is 1GHz, 200MHz, 100MHz and 50MHz. Resolutions are expressed in nanoseconds.

		100 Phe		
CRRC2 20	2,26	2,124	2,142	2,116
CRRC2 50	2,68	2,705	2,722	2,6
CRRC2 150	3,303	3,353	3,357	3,26
	50 Mhz	100 Mhz	200 Mhz	1000 Mhz
		1400 Phe		
CRRC2 20	0,606	0,579	0,585	0,581
CRRC2 50	0,715	0,721	0,723	0,719
CRRC2 150	0,895	0,895	0,894	0,893
	50 Mhz	100 Mhz	200 Mhz	1000 Mhz
		2800 Phe		
CRRC2 20	0,426	0,395	0,397	0,393
CRRC2 50	0,5	0,507	0,505	0,501
CRRC2 150	0,62	0,628	0,619	0,629
	50 Mhz	100 Mhz	200 Mhz	1000 Mhz
		5600 Phe		
CRRC2 20	0,302	0,281	0,282	0,28
CRRC2 50	0,355	0,349	0,353	0,3485
CRRC2 150	0,445	0,444	0,44	0,445
	50 Mhz	100 Mhz	200 Mhz	1000 Mhz

C Comparison of LYSO and $LaBr_3$ time properties

Mean and dispersion of the k^{t}h photoelectron arrival time for the LYSO and LaBr3 crystals

LYSO *: τ=40ns, N=2800 phe (constant N)*

photon n°	*Mean Time (ps)*	*sigma (ps)*
1	14,4	14,3
2	28,7	20,1
5	71,8	32,1
10	143,2	45,0
20	286,7	64,6
50	718,5	101,4
100	1450,3	145,2
200	2960,6	210,4
500	7861,0	354,7
1000	17664,2	564,1
2000	50084,5	1190,6

LaBr3 *: τ=16ns ; N=5600phe (Constant N)*

photon n°	*Mean Time (ps)*	*sigma (ps)*
1	2,9	2,8
2	5,7	4,0
5	14,2	6,3
10	28,6	8,9
20	57,3	12,7
50	143,3	20,5
100	287,8	29,0
200	580,8	41,2
500	1495,4	66,3
1000	3145,4	99,5
2000	7067,0	159,7
5000	35725,3	616,6

D Properties of some scintillators

	LSO	LYSO	GSO	BGO	LaBr3
Density (g/cm3)	7,4	7,1	6,7	7,1	6,3
Energy Resolution at 662 keV (FWHM)	~8%	~7.1%	~6.9%	7.9%	2.9%
Light wavelength	420 nm	410 nm	440 nm	480	380 nm
Light Yield	1.0 (27 ph/kev)	1.2 (32 ph/kev)	<0.5 (8 ph/kev)	<0.6 (9 ph/kev)	2.0 (63 ph/kev)
Decay constant time	~40 ns	~40 ns	60 ns	300 ns	16 ns
Robustess	high	high	low	high	hygroscopic

E Arrival time probability distributions of successive photoelectrons

(G. Rannuci, Nuclear Instruments and Methods in Physics Research A355, 1993)

E.1 Arrival time probability distribution for the 1^{st} photoelectron

The total number of photoelectrons is fixed to N. We want to express the probability density function of the time emission of the first photoelectron. The probability $P_1\big(N \in [t, t+\Delta t]\big)$ of finding the first photoelectron out of N within the time interval $[t, t+\Delta t]$ is the difference between

- the probability that all photoelectrons be emitted after t and
- the probability that all photoelectrons be emitted after $t + \Delta t$

The probability of occurrence of all photoelectrons after t is,[1]

$$P_1\big(N \in [t, \infty])\big) = \left(\int_t^\infty f(u)du\right)^N \tag{14}$$

We thus write

$$P_1\big(N \in [t, t+\Delta t]\big) = \left(\int_t^\infty f(u)du\right)^N - \left(\int_{t+\Delta t}^\infty f(u)du\right)^N \tag{15}$$

To simplify the expressions, we define the probability for each photoelectron to be emitted before t

$$F(t) = \int_0^t f(u)du \tag{16}$$

The expression (2) becomes

$$P_1\big([t, t+\Delta t]/N\big) = \big(1 - F(t)\big)^N - \big(1 - F(t+\Delta t)\big)^N \tag{17}$$

We develop the power of the two factors in the brackets:

$$P_1\big([t, t+\Delta t]/N\big) = \sum_{k=0}^{N} \binom{N}{k} \big(-F(t)\big)^k - \sum_{k=0}^{N} \binom{N}{k} \big(-F(t+\Delta t)\big)^k \tag{18}$$

$$P_1\big([t, t+\Delta t]/N\big) = \sum_{k=0}^{N} \binom{N}{k} (-1)^{k+1} \{\big(F(t+\Delta t)\big)^k - \big(F(t)\big)^k\} \tag{19}$$

The first term $k = 0$ being 0, the sum starts for $k = 1$. We rewrite the terms of the sum

$$\big(F(t+\Delta t)\big)^k - \big(F(t)\big)^k = \frac{\big(F(t+\Delta t)\big)^k - \big(F(t)\big)^k}{\Delta t}\, \Delta t \tag{20}$$

When the time interval Δt becomes infinitesimal, the last equation is equal to the probability of finding the first photoelectron in the infinitesimal interval $[t, t+dt]$:

$$\frac{\big(F(t+\Delta t)\big)^k - \big(F(t)\big)^k}{\Delta t} \longrightarrow \frac{d}{dt}\big(F(t)\big)^k \tag{21}$$

[1] the photoelectrons emission times are assumed uncorrelated

And the ratio probability/time interval tends to the density probability

$$\frac{P_1\big([t,t+\Delta t]/N\big)}{\Delta t} \longrightarrow p_1(t/N) \tag{22}$$

Hence, emission time probability density for the first photoelectron is written

$$p_1(t/N) = \sum_{k=1}^{N} \binom{N}{k} (-1)^{k+1} \frac{d}{dt}\big(F(t)\big)^k \tag{23}$$

This expression becomes

$$p_1(t/N) = \sum_{k=1}^{N} \binom{N}{k} (-1)^{k+1} k\big(F(t)\big)^{k-1} F'(t) \tag{24}$$

And, applying the property

$$\binom{N}{k} k = N\binom{N-1}{k-1} \tag{25}$$

By substituting eq. (12) into eq. (11) we obtain:

$$p_1(t/N) = NF'(t) \sum_{k=1}^{N} \binom{N-1}{k-1} (-1)^2 (-1)^{k-1} \big(F(t)\big)^{k-1} \tag{26}$$

We recognize that the sum is the development of the $N-1$ power of the binomial term $1-F(t)$. Finally,

$$p_1(t/N) = NF'(t)\big(1-F(t)\big)^{N-1} \tag{27}$$

We check the norm of this function:

$$\int_0^\infty p_1(t/N)dt = \big[-(1-F(t))^N\big]_0^\infty \tag{28}$$

With $F(0)=0$ and $F(\infty)=1$

$$\int_0^\infty p_1(t/N)dt = \big[-(1-1)^N\big] - \big[-(1-0)^N\big] = 1 \tag{29}$$

Finally, the explicit expression of the probability density is obtained by replacing $F(t)$ with its expression in eq. (14)

$$p_1(t/N) = N\lambda e^{-\lambda t}\big[e^{-\lambda t}\big]^{N-1} \tag{30}$$

E.2 Arrival time probability distribution for the k^{th} photoelectron

The arrival time probability density function for the k^{th} photoelectron among N can be derived from the expression (14) for the first photoelectron time distribution.

Indeed, the probability that the k^{th} photoelectron in detected the interval $[t, t+dt]$ is equal to the joint probability of 2 independent conditions:

- $k-1$ photoelectrons are detected in the interval $[0,t]$
- the first photoelectron is detected among the $N-(k-1)$ remaining photoelectrons in the interval $[t, t+dt]$

We can thus write

$$p_k(t/N)dt = \binom{N}{k-1} P\{(k-1) \in [0,t]\} p_1\big(t/(N-(k-1))\big)dt \tag{31}$$

We consider all the possible configurations of events in which $k-1$ photoelectrons out of N are emitted before time t.

The first term of eq. (18) is easy to calculate

$$P\{(k-1) \in [0,t]\} = \left(\int_0^t f(u)du\right)^{k-1} = [F(t)]^{k-1} \tag{32}$$

The second term of eq. (18) is replaced with its expression (14) with $N-k+1$ instead of N.Therefore, the probability density function of the time of emission of the k^{th} photoelectron out of N is:

$$p_k(t/N) = \binom{N}{k-1} [F(t)]^{k-1}(N-k+1)F'(t)[1-F(t)]^{N-k} \tag{33}$$

Or,

$$p_k(t/N)dt = \frac{N!}{(k-1)!(N-k)!}[1-F(t)]^{N-k}[F(t)]^{k-1}F'(t) \tag{34}$$

We again verify the norm of this function. The recursive integration by parts of the right member, $k-1$ times, gives the following equality:

$$\begin{aligned}\int_0^\infty \frac{N!}{(k-1)!(N-k)!}[1-F(t)]^{N-k}[F(t)]^{k-1}F'(t)dt \\ = \int_0^\infty N[1-F(t)]^{N-1}F'(t)dt \\ = \big[-(1-F(t))^N\big]_0^\infty = F(1)-F(0) = 1\end{aligned} \tag{35}$$

The emission time probability distribution for the k^{th} photoelectron out of N is calculated for an exponential decay function by substituting (23) and (24) in the expression (21):

$$f(t) = \lambda \cdot e^{-\lambda t} \tag{36}$$

$$F(t) = \int_0^t f(u)du = (1 - exp(-\lambda t)) \tag{37}$$

We then obtain:

$$p_k(t/N) = \frac{N!\lambda(1-e^{-\lambda t})^{k-1}}{(k-1)!(N-k)!}e^{-\lambda(N-k+1)} \tag{38}$$

F Optimal filtering principle

INTRODUCTION

Optimal filtering consists in a 2-parameter fit of a set of n samples $S_i = S(t_i)$ with a reference signal $g(t)$. The parameters, u and v, are calculated at each clock step by a linear combination of the n previous samples stored in a pipeline memory. The quality of the fit is evaluated by a χ^2 parameter. When u is above a threshold and χ^2 is minimum, the fit is good and the parameters have a physical sense: if A and τ are respectively the amplitude of the sampled signal (proportional to the energy) and its phase relatively to the reference function, then

$$S_i \approx Ag(t_i - \tau)$$

$$u \approx A$$

$$v \approx A\tau$$

DEFINITION OF THE TIME REFERENCE

The samples are written $S_i = S(t_i)$. We note t_a the pulse arrival time, defined here by the instant when the signal reaches 10% of its maximum $S(t_a) = 0.1S_{max}$. The pulse is described by a function of the variable t', whose origin is defined similarly :

$$g(t' = 0) = 0.1 \quad \text{et} \quad \max(g) = 1$$

The signal is thus written:

$$S(t) = Ag(t - t_a) + n(t), \tag{39}$$

where n is an additional noise.

The sampling is not synchronized with the beginning of the pulse:

$$S_i = Ag(t_i - t_a) + n(t_i) \quad ; \quad t_a \neq t_i$$

The optimal filter is a linear superposition of the n previous samples from S_c to S_{c+n-1}. We write $s_1 = S_d \quad ; \quad s_i = S_{c+i-1}$

Thus

$$s_i = Ag(t_{c+i-1} - t_a) + n_i \tag{40}$$

the noise is considered stationary, which means that it does not depend on the time origin. At each clock step, the shift of the samples in the pipelined memories is formally equivalent to the incrementation of the index c.

After the arrival of a pulse, there is a step for which the phase $t' = t_c - t_a = -\tau$ is minimum in absolute value, which means that the sample s_1 is close to the reference point:

$$s_1 = Ag(-\tau) + n_1$$

At this step, the parameter

$$\chi^2 = \sum_{i=1}^{n} (s_i - ug_i)^2$$

is minimum. As $t_{d+1} = t_d + \Delta t$, where $\Delta t = 1/F_e$ is the sampling period, it is clear that for this step, $-\Delta t/2 < \tau < \Delta t/2$. Indeed, any interval $[t_a - \Delta t/2, t_a + \Delta t/2]$ contains one sample.

CONSTRUCTION OF THE PARAMETERS

We consider this configuration of minimum phase to construct u and v.
The decomposition of the signal:

$$s_1 = Ag(-\tau) + n_0 \quad ; \quad s_i = Ag\big((i-1).\Delta t - \tau\big) + n_i$$

is written simply:

$$s_i = Ag(t'_i - \tau) + n_i \tag{41}$$

We write the first order limited development of $g(t)$ around each t'_i:

$$s_i = Ag(t'_i) - A\tau g'(t'_i) + n_i$$

or simply

$$s_i = Ag_i - A\tau g'_i + n_i \tag{42}$$

A and τ are estimated from linear combinations of s_i:

$$u = \sum_{i=1}^{n} a_i s_i \quad ; \quad \langle u \rangle = A \tag{43}$$

$$v = \sum_{i=1}^{n} b_i s_i \quad ; \quad \langle v \rangle = A\tau \tag{44}$$

These relations impose constraints on the coefficients:

$$u = \sum_{i=1}^{n} a_i (Ag_i - A\tau g'_i + n_i) = A + \sum_i a_i n_i$$

implies

$$\sum_{i=1}^{n} a_i g_i = 1 \tag{45}$$

$$\sum_{i=1}^{n} a_i g'_i = 0 \tag{46}$$

Similarly, for the other set of coefficients:

$$\sum_{i=1}^{n} b_i g_i = 0 \tag{47}$$

$$\sum_{i=1}^{n} b_i g'_i = -1 \tag{48}$$

At this point, we have built estimators for A and τ. Indeed, if we consider a great number of measurements for which A and τ are reproduced and only the noise n_i differs, the mean u is:

$$\langle u \rangle = \langle A + \sum a_i n_i \rangle = A + \sum a_i \langle n_i \rangle = A$$

the mean noise is zero, per definition. Similarly, $\langle v \rangle = A\tau$.

The choice of the coefficients can be optimized. Indeed, the n coefficients are constrained by only 2 equations. We use the degree of freedom to minimize the statistical error induced by noise:

$$\begin{aligned} var(u) &= var\left(A + \sum a_i n_i\right) \\ &= var\left(\sum a_i n_i\right) \\ &= \left\langle \left(\sum a_i n_i\right)^2 \right\rangle - \left\langle \sum a_i n_i \right\rangle^2 \\ &= \left\langle \left(\sum a_i n_i\right)^2 \right\rangle \quad \left(\langle n_i \rangle = 0\right) \\ &= \left\langle \sum n_i n_j a_i a_j \right\rangle \\ &= \sum_{i,j} \langle n_i n_j \rangle a_i a_j \\ &= \sum_{i,j} R_{ij} a_i a_j \end{aligned}$$

$R_{ij} = \langle n_i n_j \rangle = \rho(t_i - t_j)$ characterizes the noise autocorrelation. The values define a symmetric matrix.

The minimization of these variances must be realized while fulfilling the constraints (45) to (48). We thus introduce terms pondered by Lagrange multipliers in the function to minimize

$$I_u = var(u) - \lambda_a \left(\sum a_i g_i - 1\right) - \mu_a \sum a_i g'_i \tag{49}$$

At the minimum of this function I_u, each partial derivative is equal to zero:

$$\begin{cases} 2\sum_i R_{ik} a_i - \lambda_a g_k - \mu_a g'_k = 0 & k = 1, 2..n \\ \sum_i a_i g_i = 1 \\ \sum_i a_i g'_i = 0 \end{cases}$$

or, in terms of matrices:

$$\begin{pmatrix} R_{11} & \dots & R_{1n} & g_1 & g'_1 \\ \vdots & \ddots & \vdots & \vdots & \vdots \\ R_{n1} & \dots & R_{nn} & g_n & g'_n \\ g_1 & \dots & g_n & 0 & 0 \\ g'_1 & \dots & g'_n & 0 & 0 \end{pmatrix} \begin{pmatrix} a_1 \\ \vdots \\ a_n \\ -\lambda_a \\ -\mu_a \end{pmatrix} = \begin{pmatrix} 0 \\ \vdots \\ 0 \\ 1 \\ 0 \end{pmatrix}$$

We have omitted the factor 2. It does not impact the coefficients: only the values of the Lagrange multipliers are changed, and we are not interested in them.

Symmetrically:

$$\begin{pmatrix} R_{11} & \dots & R_{1n} & g_1 & g'_1 \\ \vdots & \ddots & \vdots & \vdots & \vdots \\ R_{n1} & \dots & R_{nn} & g_n & g'_n \\ g_1 & \dots & g_n & 0 & 0 \\ g'_1 & \dots & g'_n & 0 & 0 \end{pmatrix} \begin{pmatrix} b_1 \\ \vdots \\ b_n \\ -\lambda_b \\ -\mu_b \end{pmatrix} = \begin{pmatrix} 0 \\ \vdots \\ 0 \\ 0 \\ -1 \end{pmatrix}$$